

Chapter 1

Introduction to the Research

1.0: Introduction

This dissertation deals with the subject of plasma flow damping in stellarator configurations with and without quasi-symmetry. This subject is one small area of research in the broad quest for fusion energy. It is the purpose of this chapter to summarize the results and place them in a broader context.

Section 1 of this chapter describes the need for fusion energy, briefly summarizes the progress that has been made toward that goal, and introduces the concept of the stellarator. Section 2 provides technical details about the HSX stellarator. A review of relevant previous research is given in Section 3. A summary of the contents of this dissertation is provided in Section 4.

1.1: Fusion Power and the Machines that May Generate It

Measurements have shown that the CO_2 concentration in the atmosphere has increased from ≈ 280 ppm to ≈ 380 ppm since the advent of industrialization, and projections indicate that it will continue to grow unless stabilization policies are adopted.¹ While there are still large uncertainties in the modeling, it is predicted that this CO_2 concentration increase will have a major impact on the Earth's climate. For instance, stabilization of the CO_2 concentration at 550 ppm is projected to lead to a global temperature rise of ≈ 2 C and a sea level rise of ≈ 1 meter,² inundating low lying areas and causing vast economic disruption.¹

To avoid a runaway CO_2 concentration, it is necessary to reduce future emissions. CO_2 emission profiles required for eventual stabilization at different concentrations have been calculated and are shown in figure 1.1. The solid (WRE, by Wigley, et al.²) and dashed (IPCC, Intergovernmental Panel on Climate Change) curves represent different economic scenarios for the projections, but they agree that stabilization of CO_2 at less than 1000 ppm level will eventually

require a significant reduction in CO₂ emission. For reference, the emission in an unconstrained scenario (IS92a) is also shown.

These constraints on emission are coupled to growing requirements for electric power generation throughout the world. Assuming that each person in the world uses 3kW of power on average (about ¼ the amount used by the average US citizen in 1999), and assuming that the earth's population grows to 10 billion people by 2050, the required power generation will be ~30 TW.³ This should be compared to the 2002 level, when world wide primary power generation was ~13 TW, of which ~85% is fossil fueled.³ It will be necessary to reduce carbon emissions significantly while making large increases in total generation. In particular, projections have indicated that between 10 and 30 TW of carbon free power will be necessary by 2050 for the stabilization of atmospheric CO₂ in the 450-750 ppm range.⁴

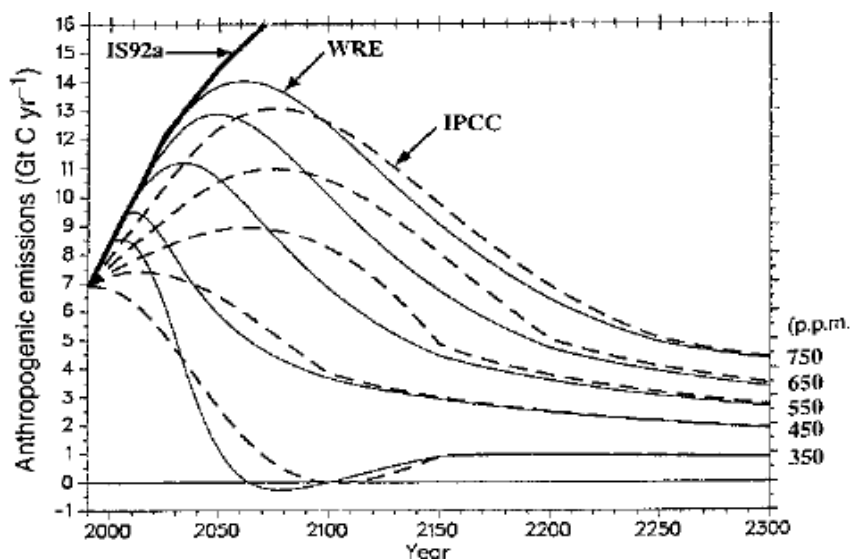


Figure 1.1: Estimates of Different CO₂ emission scenarios required to stabilize atmospheric CO₂ concentrations at 350, 450, 550, 650, and 750 ppm. Figure from T.M.L. Wigley, et. al.

There are a number of technologies which have been considered for the solution of this problem, including large scale sequestration of CO₂ underground or in the deep oceans, wind power, solar power, and nuclear fission.⁵ Another potential solution to this problem lies in the

promise of controlled nuclear fusion for energy production. In this process, the nuclei of atoms collide with sufficient energy that they join, releasing energy in the process. Unfortunately, the energies at which these reactions occur are such that matter cannot exist in solid, gas or liquid form. The reacting elements are in the form of a plasma, a soup of colliding electrons and atomic nuclei. When this ionized gas is heated to the appropriate temperature (≈ 10 keV for a plasma made up of equal parts of the hydrogen isotopes tritium and deuterium), the colliding nuclei fuse and release energy in the reaction.

If this plasma were unconfined, it would quickly expand into whatever volume enclosed it, touching material surfaces and cooling to temperatures where fusion reactions no longer occur. Hence, it is necessary to hold the gas away from the material surfaces of the containment vessel. One solution to this problem is based on the observation that charged particles in a magnetic field are like beads on a string: the particles can free-stream along the magnetic field, but their motion across the magnetic field is significantly impeded.⁶ If magnetic fields can be arranged in a toroidal (doughnut shaped) geometry where the field lines close on themselves without intersecting material surfaces, then the plasma will ideally be well confined away from the chamber walls. Continuing the bead analogy, a toroidal magnetic confinement system is like a bead on a rigid hoop.

Experiments in fusion machines have demonstrated that the magnetic field does not perfectly confine the heat and particles of the plasma; combinations of turbulence and collisions between particles cause heat and particles to be transported across the magnetic field to the material surfaces of the chamber. The time scale over which the heat is lost is called the energy confinement time, τ_E . For a fusion power plant to be self sustaining, the plasma must be sufficiently hot, dense, and well confined. This requirement is manifested in the so called fusion triple product.⁷ For ion temperatures near the maximum cross section for deuterium-tritium (D-T) fusion, this requirement can be written as

$$nT\tau_E > 5 \times 10^{21} \text{ m}^{-3} \cdot \text{keV} \cdot \text{s}$$

where n is the plasma density, and T is the plasma temperature. Note that nT is the plasma pressure. The product of the pressure and confinement time must be sufficiently large for a sustained reaction to occur. Satisfying this requirement has been the major goal of fusion research to date.

The present generation of large fusion experiments is close to reaching this goal. The JET tokamak with a D-T mixture has achieved a transient ratio of fusion power to heating power ($Q=P_{\text{fusion}}/P_{\text{input}}$) of 0.6⁸ and steady state discharges with $Q=0.22$.⁹ Other D-T plasmas in JET have transiently achieved a fusion triple product of 10^{21} keV·m⁻³·sec.¹⁰ Values of the fusion triple product of 3.1×10^{20} keV·m⁻³·sec have been achieved in the JT-60 tokamak under full non-inductive current drive by a careful tailoring of profiles.¹¹

The results quoted above are from a type of fusion machine known as a tokamak. In this configuration, a large current is driven in the plasma, creating part of the magnetic field which confines the plasma. Maintaining this current in steady state is a substantial technical challenge. A second class of fusion machines, known as stellarators, generate all or most of the confining magnetic fields via external coils, and are thus inherently steady state.

Unfortunately, traditional stellarators have been at a disadvantage to tokamaks with respect to transport. Neoclassical transport is the enhancement over classical collisional transport⁶ caused by the inhomogeneities in the strength of the magnetic field.¹² In an axisymmetric system such as a tokamak, the magnetic field is stronger on the inside of the torus than the outside. This can be seen in the expression for the magnetic field:

$$\mathbf{B} = \frac{B_0}{1 + \varepsilon \cos(\theta)} (\Theta(r) \mathbf{e} + \mathbf{o}) \quad (1.1)$$

In this expression, $\Theta = \varepsilon/q(r)$ and $\varepsilon = r/R_0$ where $q = rB_t/RB_p$ is the safety factor. θ is the poloidal angle, corresponding to the short way around the torus, and \mathbf{e} is a unit vector in the poloidal direction. The long way around the torus is the toroidal direction; $\mathbf{\varphi}$ is a unit vector in this direction. Some particles are reflected from the high magnetic field region of the torus by the

magnetic mirror effect.¹³ The net effect of this bouncing in the two dimensional magnetic field is a diffusion coefficient that scales like $D \sim \nu \rho^2 q^2 / \epsilon^{3/2}$. This expression is a factor of $q^2 / \epsilon^{3/2} \sim 3^2 / 2^{3/2} \sim 100$ larger than the classical diffusion coefficient ($D_c \sim \nu \rho^2$), although the dependencies on gyroradius and collision frequency are identical to the classical case.

Even though the collisional transport is increased in a tokamak compared to the classical value, the situation is still not so bad. All particle orbits are still confined to the system except at the very edge.¹⁴ The magnetic field asymmetry in the poloidal direction will damp poloidal flows on an ion-ion collision time, but the symmetry of the system in the toroidal direction allows plasma to flow in that direction without any neoclassical damping. Neoclassical currents¹⁵ which result from the magnetic field inhomogeneity will play a critical role in sustaining the plasma current in steady state tokamaks. In general, the rate at which heat, momentum, and particles are lost from tokamaks is significantly larger than the neoclassical prediction. Observations indicate that apart from some exceptional circumstances,¹⁶ turbulent transport dominates the rate at which heat and particles are lost from the system.^{17,18,19}

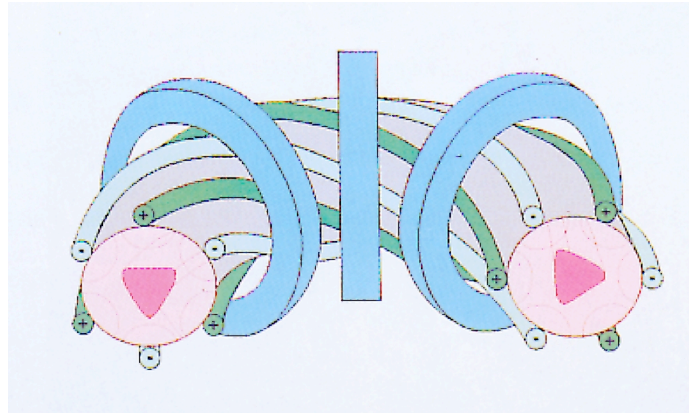


Figure 1.2: A representation of the coils and plasma shape for a typical conventional stellarator.²⁰

In a traditional stellarator like that shown in figure 1.2, the structure of $|B|$ on a magnetic surface is more complicated than in the case of a tokamak. In general, the decomposition of $|B|$ in

Fourier harmonics results in a very large number of terms (α is the poloidal angle and ζ is the toroidal angle):

$$B = B_o \left[1 + \sum_{n,m>0} \varepsilon_{n,m} \cos(m\alpha - n\zeta) \right] \quad (1.2)$$

If two or more terms in the sum are not zero (and not of the same helicity), then the direction of symmetry is lost. This loss of symmetry will lead to strong neoclassical damping of flows in all directions on a flux surface.²¹ The particle drifts in the stellarator field are much more complicated than the tokamak case, and lead to a situation where the diffusion coefficient actually increases as the collision frequency decreases.²² Furthermore, the diffusion coefficient in a stellarator is itself a function of the electric field. The electrons and ions diffuse at different rates until the electric field adjusts itself to a value such that the fluxes are balanced.²³ It was thought in the past that these bad neoclassical transport properties made the stellarator an unacceptable candidate for a fusion reactor.

Theoretical work in the 1980's has added new insight into methods to eliminate the bad stellarator neoclassical transport. One early paper considered the diffusion coefficient in a stellarator field where the helical spectral component had a poloidal modulation:

$$B = B_o \left[1 - \varepsilon_T \cos(\alpha) - \varepsilon_H \cos(m\alpha - n\zeta) (1 - \sigma \cos(\alpha)) \right], \quad (1.3)$$

It was demonstrated that for $\sigma=1$, the drift of a trapped particle off of the flux surface was reduced for most particles compared to the $\sigma=0$ case, but that $\sigma=-1$ increased the drift.²⁴ With this observation, it became clear that it is possible to reduce stellarator neoclassical transport by tailoring the magnetic field structure. This idea of "drift optimization" is present in varying degrees in the design of both LHD and W7-X.²⁵

It was next observed by Nührenberg and Zille that a class of stellarators could be found which had high MHD stability limits; these stellarators became known as "Helias".²⁶ In this research, the configuration was purely specified by the boundary shape and plasma profiles. This approach allowed more accurate targeting of physics properties, instead of initially specifying a

coil configuration and then examining the physics properties after the fact. It was later observed that a subset of this class of stellarators has a magnetic field spectrum which was dominated by a single helical component.²⁷ In this case of “quasi-helical symmetry”, the direction of symmetry was restored; in this case, there is a helical path along the torus where $|B|$ does not change. This quasi-helically symmetric configuration had neoclassical transport levels similar to a tokamak. It was further shown that these configurations can have a magnetic well at $\beta=0$ and smaller parallel currents than a conventional stellarator, both of which are beneficial for operation at high β (β =ratio of plasma pressure to magnetic field pressure).

The final necessary step was to develop a method to generate physical coils for these stellarators. This problem was solved by Merkel,²⁸ who developed a method to generate currents on a winding surface outside the plasma boundary, based on the specified plasma configuration. Once the currents on this winding are discretized into actual coils, the problem is conceptually solved. This is the conceptual process which lead to the HSX stellarator.

Since that time, other types of quasi-symmetry have been developed. Designs with quasi-toroidal symmetry have been developed,²⁹ and the National Compact Stellarator Experiment (NCSX)³⁰ is an example of a machine with this symmetry. Stellarators with quasi-poloidal symmetry have also been designed, of which the QPS stellarator is an example.³¹

1.2 The HSX Stellarator

The Helically Symmetric eXperiment (HSX)³² is the world's first quasi-symmetric stellarator. In a Fourier decomposition of $|B|$ in Boozer toroidal (ζ_B) and poloidal (α_B) angles,³³ the field is represent as

$$B = B_o \sum_{n,m} b_{nm} \cos(n\zeta_B - m\alpha_B) \quad (1.4)$$

The magnetic field spectrum in Boozer coordinates in HSX is shown in the left frame of figure 1.3, for the base quasi-helically symmetric (QHS) configuration. The spectrum is dominated by the

single $(n,m)=(4,1)$ helical spectral component. In a traditional stellarator, an $(n,m)=(0,1)$ spectral component would be present in addition to the helical component, with amplitude equal to the inverse aspect ratio of the particular surface ($b_{0,1} \approx -r/R$). In HSX, this component is suppressed to the extent that based upon the magnitude of this component, the inferred aspect ratio of HSX would be ≈ 400 , even though the physical aspect ratio is ≈ 10 . The large reduction of toroidal curvature has been experimentally verified by inspecting the orbits of passing particles.³⁴ Hence, HSX looks like a straight stellarator, even though it is in toroidal geometry.

The right hand frame of figure 1.3 illustrates the small components of the magnetic field spectrum which lead to breaking of the quasi-symmetry. Some of the terms $(12,3)$ and $(8,2)$ have the same helicity as the main $(4,1)$ spectral component. A $(48,0)$ term is also present, representing the ripple due to the finite number of coils in HSX. Note that in general, the terms with $m=0$ are finite at the magnetic axis, while the $m \neq 0$ terms go to zero on axis. A detailed discussion of the magnetic field spectrum will be presented in chapter 5.

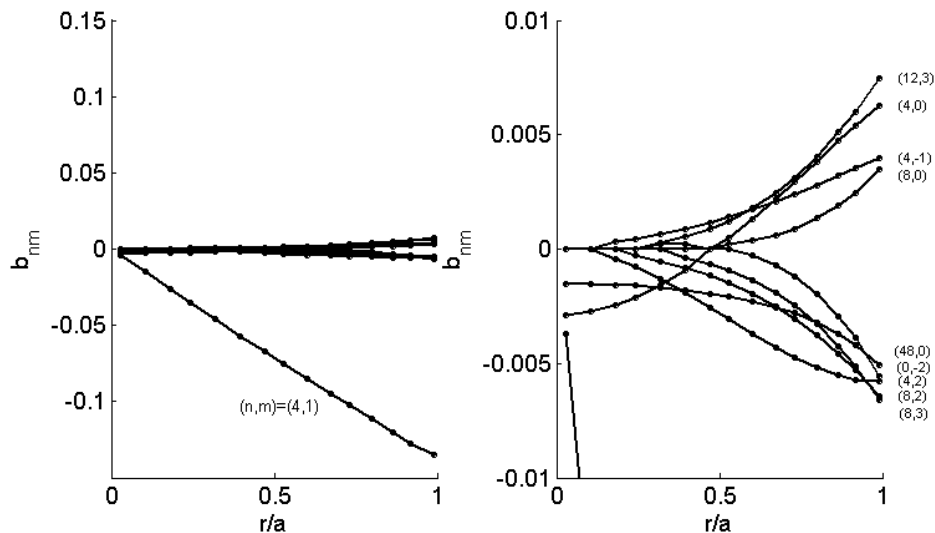


Figure 1.3: The Boozer spectrum of the HSX stellarator (left), and the details of the small symmetry breaking components present in the spectrum (right). Note the different scales.

The special magnetic field of HSX is produced by a set of 48 modular, non-planar coils, as illustrated in the 3-D view of the machine in figure 1.4. The basic unit building block of each

coil is a bundle of six 8mm x 8mm copper conductor, double wrapped in Kevlar to form a winding pack. This winding pack is used to form the 14 turns of each coil; in particular, from 2 pancakes of 7 turns in each pancake. The entire coil is potted in epoxy to give it strength to hold its shape. The coils are fed with coaxial current feeds and closely separated parallel plate bus work, specially designed to reduce error fields.

Adjacent to each of these non-planar coils is a 10 turn planar coil. These coils can be used to modify the machine configuration. In particular, a second large term in the $|B|$ spectrum with mode numbers $(n,m)=(4,0)$ can be excited in the "Mirror Mode" configuration. In this case, the neoclassical transport properties are degraded back to the level of a conventional stellarator. This particular configuration of HSX will be discussed in great detail in later chapters. The auxiliary coils can also be used to vary the magnetic well depth and rotational transform. A detailed study of the configuration space accessible in HSX is presented in Appendix 2.

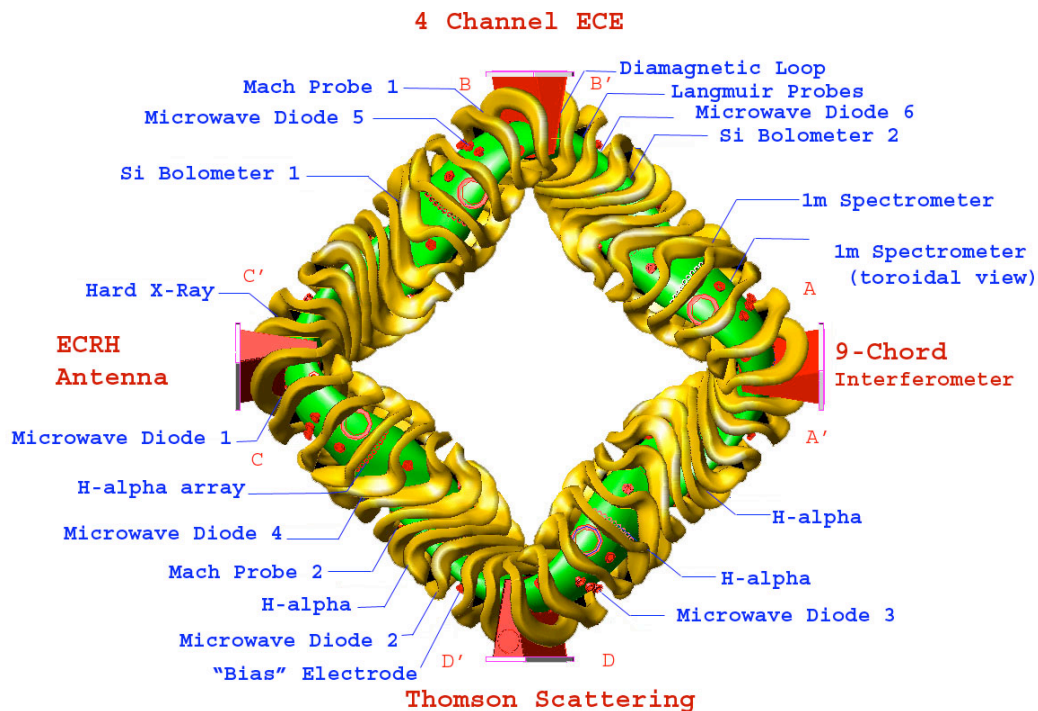


Figure 1.4: The HSX modular coils and the diagnostic set. Figure courtesy of J. Radder and K. Likin.

Figure 1.4 also illustrates the approximate diagnostic layout on HSX. The stored energy is diagnosed with a diamagnetic loop. The plasma density is monitored with a nine chord microwave interferometer operated in collaboration with UCLA.³⁵ The absorption of microwaves is determined using a set of microwave diodes spaced around the torus.³⁶ Electron temperature is diagnosed with either a Thomson scattering system or a multi-channel ECE radiometer, although these diagnostics were not available when the data presented in this dissertation was collected. Radiated power is measured using UV-enhanced silicon photodiodes. The 1-meter spectrometer, H_{α} arrays, biased electrode, and Mach probes are the tools and diagnostics designed and constructed for the purpose of this dissertation, and will be described in later chapters.

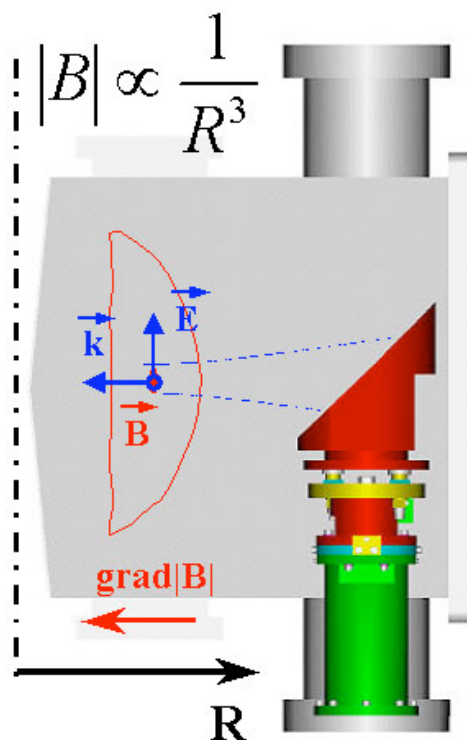


Figure 1.5: The ECH launching system on HSX. The magnetic field is mostly out of the page in this view. Figure courtesy of K. Likin.

Plasmas are produced and heated in HSX using electron cyclotron heating at $B=0.5T$ with a 28 GHz gyrotron. The radiation is transported from the gyrotron to the torus via a system of waveguides and mode converters.³⁷ After passing into the vacuum vessel through a quartz

window, the microwave power is reflected off of an ellipsoidal focusing mirror into the plasma from the low magnetic field side of the torus. The launched polarization is X-mode for all data presented in this dissertation, although O-mode polarization is also possible by rotating one of the mode converters. The focused microwave beam has a spot size of approximately 4cm at the magnetic axis. An illustration of the launching system is given in figure 1.5. Important machine parameters are given in table 1.1.

Field Periods	4
Main Modular Coils Per Field Period	12
Auxiliary Planar Coils Per Field Period	12
Coil Current for QHS Central ECH Resonance	5361 A main coils, 0 A aux. coils
Magnetic Field at Resonance	0.5 Tesla (2 nd Harmonic always)
ECH Power	Up to 100kW launched.
Magnet Pulse Flat-Top Duration	≈0.2 seconds.
ECH Pulse Length	Up to .050 seconds
Base Pressure	1×10^{-8} to 5×10^{-8} torr
Vacuum Conditioning Techniques	Helium glow discharge cleaning.
Working Gasses	H ₂ , D ₂ , He
Possible Line Average Densities	1×10^{11} to 2.5×10^{12} cm ⁻³

Table 1.1: Major parameters of the HSX device.

Typical plasma parameters for HSX are illustrated in table 1.2. These parameters are typical of a location at $r/a \sim 0.6$ in discharges with a line average density of 1×10^{12} cm⁻³. They would vary with location in the plasma, and are only meant to be representative of typical parameters.

B	0.5 T
n_e	1×10^{18} m ⁻³
T_e	200 eV
T_i	20 eV
ω_{ce}	88×10^9 1/s
ω_{ci}	48×10^6 1/s
ω_{pe}	40×10^9 1/s
v_{te}	8.4×10^6 m/s
v_{ti}	62×10^3 m/s
r_{Le}	7×10^{-5} m
r_{Li}	1×10^{-3} m

Table 1.2: Parameters of the HSX plasma.

1.3 Review of Previous Results

The work performed for this dissertation is based upon the results of ~50 years of previous research. This section will present a sampling of the previous results which are relevant to the current work. The relationship between plasma flows, electric fields, and enhanced confinement modes will be described. With this motivation for the importance of plasma flow studies, a review of experimental momentum transport results will be provided.

Since the discovery of the H-mode in the ASDEX tokamak in 1982,³⁸ enhanced confinement regimes have been a topic of intense experimental and theoretical interest. These ASDEX discharges are an example of an edge transport barrier (ETB) called a high mode or H-mode. The H-mode is characterized by sharpening of the edge density and temperature gradients, reduction of recycling, increases in plasma density and stored energy, and reduction of edge turbulent fluctuation amplitudes. H-modes have occurred in every auxiliary heated divertor tokamak in operation since 1982,³⁹ and are the reference scenario for operating the large tokamak experiment ITER.⁴⁰ When the region of improved confinement and reduced transport occurs internal to the plasma, it is referred to as an internal transport barrier (ITB).⁷ Both internal and edge transport barriers have been observed in tokamaks and stellarators.

As an explanation of this seemingly universal enhanced confinement phenomenon, the paradigm of **ExB** flow shear has emerged. In this paradigm, the shear in the **ExB** flow causes decorrelation of the turbulence, reducing the level of turbulent transport. It is not simply the bulk plasma flow that improves the confinement, but the **ExB** drift. This has been clearly demonstrated in high- T_i mode discharges in Heliotron-E,⁴¹ and in comparisons of ITB discharges in TFTR and DIII-D.⁴² As noted in the review by Burrell,³⁸ all particles are subject to the **ExB** drift regardless of the turbulent mode. In particular, for electrostatic flute-like modes, the **ExB** term is the only convective term.⁴³ Hence, the **ExB** flow has a special place in the paradigm.

The radial electric field must be consistent with the radial force balance equation:

$$E_r = \frac{\nabla_r p}{en} - v_\theta B_\varphi + v_\varphi B_\theta \quad (1.5)$$

This equation illustrates that the radial electric field is determined by some combination of the pressure gradient and the plasma flows. Furthermore, there are complex feedback cycles at play. Changing the flows will change E_r , which could in turn change the transport properties and hence the pressure gradient. This could in turn effect the flows and electric field. The important physics point is to resolve for any given confinement regime which terms in (1.5) determine E_r , and how the balance changes in time.

As an example of this balance, there is observed to be a fast increase in the edge poloidal rotation before the transition to H-mode in DIII-D.⁴⁴ This poloidal rotation excursion gives rise to a radial electric field at the edge before the edge pressure changes. After the transition, the edge pressure gradient grows and eventually balances the electric field.⁴⁵ A similar transition was observed during the enhanced reverse shear transition in TFTR, with a fast excursion in poloidal velocity,^{46,47} followed by a pressure gradient balancing the electric field in the region of improved confinement.

On the other hand, in some internal transport barrier discharges in DIII-D, the radial electric field is dominated by the toroidal rotation term in the radial force balance.⁴⁸ These discharges are heated with co-directed NBI, leading to a strongly positive electric field in the center, and in some cases have been able to achieve neoclassical levels of ion transport across the entire plasma.¹⁶ This is in contrast to internal transport barriers achieved with counter-NBI, where the toroidal rotation is the same sign as and dominated by the pressure gradient term in the radial force balance.⁴⁹ These discharges generally have a broader pressure profile and the associated enhanced stability.⁵⁰ A second class of discharges with counter-NBI is the so-called quiescent double barrier (QDB) mode, where transport barriers are found in both the core and edge.⁵¹ In both regions of improved confinement, the negative electric field is supported by the pressure gradient. In QDB discharges, there is a zero crossing of the \mathbf{ExB} shearing rate, causing

the edge and core barriers to be separated by a region of non-improved transport. The merging of these barriers causes high performance¹⁷ at the expense of MHD stability,⁵² and the separation between the barriers in the QDB regime may be responsible for the steady state nature of these regimes.

Internal transport barriers have been observed in stellarators as well. One example is the High Ion Temperature (HIT) modes in Heliotron-E⁴¹ and CHS.⁵³ In both of these machines, this mode is obtained under low recycling conditions in low density NBI plasmas. In both cases, a target ECH plasma is made, and the externally controlled gas feed is turned off as soon as the NBI begins. The strong central fueling from the NBI and low recycling lead to a highly peaked electron density profile, and a doubling of the central ion temperature. In the Heliotron-E case, it was shown that the ion pressure gradient supports the electric field in these cases. This enhanced confinement mode probably has its closest tokamak analogy with TFTR "supershots".⁵⁴ This tokamak enhanced confinement regime was observed in low density balanced-NBI discharges after thorough limiter conditioning to reduce the influx of hydrogen from the walls.

Besides these examples of spontaneously occurring transport improvements, experiments in the CCT tokamak demonstrated that it is possible to stimulate an H-mode by externally imposing an electric field on the plasma.⁵⁵ In these discharges, a large probe is inserted into the edge plasma inside the last closed magnetic surface and biased to some large voltage. The electrode collects current from the plasma and charges up the magnetic flux surface on which it resides; this has the effect of externally imposing an electric field on the plasma edge. A bifurcation in the edge profiles is often seen, with an improvement in particle confinement and a reduction of edge turbulence. It has been demonstrated in TUMAN-3⁵⁶ and TEXTOR⁵⁷ that these "biased" H-modes can occur for either polarity of the electric field, even though the "natural" H-modes always have an E_r well at the edge. Hence, the sign of the electric field is not the critical parameter in triggering the transition, but rather the magnitude and \mathbf{ExB} shear. Other examples of biased H-modes have been seen in T-10⁵⁸ and Phaedrus-T.⁵⁹ It has also been found that biasing

a limiter or the separatrix of a plasma can improve confinement or reduce the H-mode power threshold, without the insertion of a material object inside the separatrix.⁶⁰

Having established that electric fields are critical components of enhanced confinement in both stellarators and tokamaks, and that plasma flows are intimately connected to electric fields, it makes sense to inquire about the physical mechanisms of plasma flow damping. As alluded to in Section 1.1, magnetic field inhomogeneities cause viscous damping of plasma flows. This will be the general subject of this dissertation. However, it has been found that in a large variety of situations, neoclassical transport is insufficient to account for the observed flow damping. In some cases, the enhanced flow damping appears to be due to electrostatic turbulence; other cases indicate the importance of magnetic activity in momentum damping.

The damping of toroidal flows in tokamaks has been extensively studied. Some of the first work in this area was performed on the Princeton Large Torus (PLT).^{61,62} These early experiments were performed using co- or counter- directed neutral beam injection (NBI) to apply torque to the plasma, while measuring the Doppler shift of light emitted from highly ionized states of intrinsic impurities to deduce the plasma rotation. Toroidal rotation speeds of $\sim 10^5$ m/s were measured for ~ 500 kW of injected beam power. The beam torque and rotation speed lead to a momentum confinement which was a factor of 10 smaller than the anticipated charge exchange rate and significantly smaller than the damping due to toroidal field ripple. Hence, it was inferred that the momentum transport was anomalous. A simple momentum balance was done using a momentum diffusivity $\propto 1/n$ and a measured estimate of the beam torque, illustrating that the spin-up and spin-down times were consistent with the measured steady state flow speed.

Work on the ISX-B tokamak with unbalanced and balanced beam injection continued these types of studies.⁶³ There had been concern that the large rotation induced by unbalanced neutral beam injection might lead to confinement degradation.^{61,63} It was observed that the toroidal rotation saturated as the neutral beam power was increased, implying the presence of a power degradation in momentum confinement. Hence, it was inferred that plasma rotation was

not the cause of the observed degradation of energy confinement with increasing neutral beam power. On the other hand, the observed momentum confinement times were on the order of the energy and particle confinement times. A model for the momentum damping based on gyroviscosity⁶⁴ predicted a momentum confinement time which was consistent with the measurements.

Similar results were reported from the Doublet-III tokamak. Using an early CXRS⁶⁵ system, it was observed that in unbalanced NBI divertor discharges, the D-III plasma rotated as a rigid body, and that different impurity species had the same toroidal rotation speed. Power and momentum balance analysis showed that the confinement times for energy (τ_E) and for momentum (τ_ϕ) had similar magnitudes and the same scaling with plasma current and beam power in most discharges. This implies some similarities in the underlying transport mechanisms. On the other hand, the current scaling of the momentum confinement time was found to be incommensurate with the gyroviscosity model mentioned above. Results similar to these were obtained on ASDEX.⁶⁶ Results on JET during this period also indicate the similarity between ion thermal and momentum transport in discharges without large magnetic activity.⁶⁷ It was also noted in Doublet-III that some discharges without sawteeth also show no significant plasma rotation. The relationship between τ_ϕ and τ_E noted above appears to break down in this case; large stationary magnetic islands were considered as a possible cause of this rotation damping.

Detailed measurements of toroidal momentum transport were made in TFTR.^{68,69} As in previous studies, ion energy and momentum were deposited by NBI and the ion rotation and temperature profiles were determined by the CXRS system. Transport analysis was done on these two ion channels, yielding profiles of the effective heat (χ_i) and momentum (χ_ϕ) diffusivities (effective in the sense that convection terms were not included in the heat and momentum balance). It was found that to within a factor of two, χ_i and χ_ϕ had the same numerical values and profile shapes. This result has been very significant, as a certain class of instabilities called ion temperature gradient (ITG) modes is anticipated to yield $\chi_i \approx \chi_\phi$.⁷⁰ These instabilities are expected

to grow when the gradient parameter $\eta_i = \nabla \ln(T_i) / \nabla \ln(n_i)$ exceeds a critical value (η_c). An evaluation of the η_i based on the measured profiles in TFTR indicates that it tends to stay near a critical value η_c predicted by theory, above which strong ITG turbulence would cause large radial transport. The implication is that the profiles are only marginally stable to ITG turbulence. On the other hand, the unity ratio of momentum to heat diffusivities was shown to be incommensurate with neoclassical transport, even in the unlikely case that some large unknown field error was the sole source for the momentum damping.

These studies have been continued in DIII-D, where a very large database of discharges (10 years worth) has been analyzed to determine the relationship between momentum and energy transport.⁷¹ In this work, simple replacement times for the angular momentum and heat were defined, and the ratio of those times is shown to be proportional to the ratio of the rotation frequency to the ion temperature. For 56,000 time slices where this analysis had been performed, it was found that the ratio of the replacement times in the plasma core was equal to 0.99 with a standard deviation of 0.34. The ratio differed slightly from unity for chords passing inside or outside of the magnetic axis. This database included discharges with H-mode and L-mode edges, internal transport barriers (ITBs) and various other features, displaying the universality of the relationship between momentum and heat transport. These results also provide a mystery: in many of the ITB discharges, the ion thermal transport was near the neoclassical level. Yet if all ion transport channels were neoclassical, then $\chi_\phi / \chi_i \sim 10^{-2}$. This is not consistent with the data, illustrating that momentum transport is still not fully understood.

In addition to the measurements of anomalous momentum diffusion described above, there have been measurements of momentum convection in tokamaks. In JT-60, an inward pinch of momentum was observed using a modulated-NBI technique.⁷² After the transition to the EDA (enhanced D_α) H-mode in Alcator C-Mod, toroidal momentum is observed to propagate from an unknown source at the edge to the core, leading to a flat rotation profile.⁷³ This observation can be described by diffusion of momentum generated at the edge by the unknown source. In ELM-

free H-modes, there is a rapid increase of the toroidal rotation after the transition to improved confinement, ending with a peaked toroidal rotation profile. Given that there is no core momentum input, the phenomenon must be due to a momentum pinch.

It should also be noted that momentum transport can be related to magnetic activity. Experiments in JET⁷⁴ and MST⁷⁵ indicate the importance of MHD mode coupling as a means of transferring angular momentum between different flux surfaces and the wall. As this mechanism does not appear to be relevant to a low β , quiescent HSX plasma, it will not be discussed here further.

In addition to the H-mode studies noted above, biased electrode experiments in axisymmetric systems have studied the physics of momentum damping. The biased electrode causes a current to flow through the plasma across the magnetic surfaces. This current causes a $\mathbf{J} \times \mathbf{B}_p$ torque in the toroidal direction. For a perfectly axisymmetric tokamak, there is no viscous damping of toroidal flows due to neoclassical parallel viscosity. The toroidal force and small damping imply that the plasma toroidal rotation should run away to a very large value. In contrast to this prediction, the toroidal rotation during the electrode biased phase is often quite small,⁷⁶ implying that there must indeed be significant damping of toroidal rotation.

Various models have been proposed to account for this rotation damping. Rozhansky and Tendler have suggested a model involving anomalous momentum diffusivity.⁷⁷ Under this assumption, and assuming that there are no large gradients in the poloidal rotation (the L-mode) they have derived an expression for the radial conductivity that approximately matches the L-mode data from the tokamak TUMAN-3.⁵⁶ Comparisons will be made between this model and HSX data in Section 7.1. Alternatively, Cornelis et.al.,⁷⁸ have a model for the TEXTOR biased electrode experiments where ion-neutral friction damps the toroidal flow sufficiently to account for the observed radial current. In biased electrode experiments on an RFP, measurements have indicated that the large radial conductivity may be due to magnetic fluctuations.⁷⁹

Damping of flows in stellarators has been studied less exhaustively. Experiments in CHS were done using NBI to drive rotation and a CXRS system to measure the resulting plasma flow. In CHS the amount of neoclassical viscous damping (the neoclassical toroidal viscosity) near the axis could be increased (decreased) by shifting the flux surfaces out (in), yielding a degree of control in the experiments. In all cases, the neoclassical toroidal viscosity increases by one to two orders of magnitude towards the edge. The measured toroidal rotation profiles showed that the toroidal flow went to zero toward the edge, consistent with the large toroidal viscosity there. With regards to the core rotation, an effective viscosity coefficient μ_{eff} was defined, which was proportional to the ratio of the beam torque to the central flow speed. In configurations where the neoclassical damping was large, this parameter had a near neoclassical value. When CHS was run in configurations with smaller field ripple, the effective damping coefficient was observed to be much larger than the neoclassical prediction, and it was thus inferred that some anomalous perpendicular viscosity was present. In these anomalous regimes, the density scaling of μ_{eff} was similar to LHD scaling,⁸⁰ which represents well the anomalous energy transport in CHS.

Biased electrode experiments in small stellarators have provided some insights into neoclassical viscous damping of flows. Experiments in the IMS stellarator⁸¹ provided a clear example of the competition between neoclassical viscosity and ion-neutral friction. In the core of the plasma where the viscous damping due to field ripple was reduced, the plasma flow damping and radial conductivity was dominated by ion-neutral friction. Toward the plasma edge, where the magnetic field ripple was larger, damping due to neoclassical viscosity became the dominant effect. These observations are in approximate agreement with the predictions of the model by Coronado and Talmadge.⁸²

An interesting effect due to poloidal viscosity in stellarators has been observed in the context of the H-mode transition. In W7-AS, H-mode access is only available in a few configurations with the edge rotational transform lying in small windows surrounding $\iota_a=0.48$, 0.53, and 0.57.⁸³ On the other hand, the H-mode is present in both NBI and ECH heated

plasmas, indicating that the magnetic field topology is the important feature.⁸⁴ This unique feature in W7-AS has been explained by neoclassical viscous damping.⁸⁵ In the configurations with H-mode access, the edge of the plasma is determined by the inner separatrix of natural island chains ($t_a=5/9, 10/19, \text{ and } 10/21$), but there are no island chains with $n=5$ or $n=10$ inside the LCFS. When these islands are inside the LCFS, they cause a strong corrugation of the surfaces, leading to enhanced viscous damping. When these islands are sitting outside the LCFS, the surfaces have a smooth shape. This results in a minima of the poloidal damping, allowing poloidal spin-up and the associated E_r shear. Similar H-mode windows may also have been found in Heliotron-J.⁸⁶

In summary, the results presented above illustrate the importance of plasma flows and electric fields in understanding the level of heat and particle transport in toroidal magnetic confinement systems. Furthermore, the results show that in general, the damping of plasma flows is not a well understood physical phenomenon. Both anomalous and neoclassical flow damping mechanisms appear to be important.

1.4: Summary of this Work.

The purpose of this research is to make a first study of the plasma flow damping and radial conductivity in a quasi-symmetric stellarator. The overall scheme is to induce plasma flow using a fast switching biased electrode. We have used Mach probes to measure the plasma flow and floating potential measurements to ascertain the evolution of the electric field. These measurements allow a determination of the plasma flow directions and time scales, which can then be compared to extensive neoclassical modeling.

The probe and electrode tools used in this work are discussed in chapter 2. The biased electrode is a 0.75" diameter disk of molybdenum which is inserted inside the last closed magnetic surface and biased with respect to the vessel wall to very high voltages. The power supply has been designed using fast switching insulated gate bipolar transistors (IGBTs); at turn

on, the voltage is applied in $\sim 1\mu\text{s}$, while the current is broken in $\sim 1-2\mu\text{s}$ at turn off. The response of the plasma to the electrode bias is characterized using a set of multi-tipped Mach probes, known as "Gundestrup Probes".⁸⁷ The probes implemented on HSX have six tips facing outward from the body of the probe, allowing a determination of the plasma flows in the flux surface. The probes also have a seventh pin which is used to measure the local floating potential. The electrode voltage and current and Mach probe data are measured with $>100\text{kHz}$ bandwidth, allowing observation of fast changes during the electrode voltage pulse.

It is necessary to know the ion temperature for calculating the neoclassical viscosity and the neutral density for estimating the ion-neutral friction contribution to the plasma flow damping. The spectroscopic diagnostics which make these measurements are described in chapter 3. Two arrays of H_α detectors have been placed on HSX; one array is distributed toroidally around the machine, while the other is at a fixed toroidal angle at the location of the gas puffer. These two arrays allow the monitoring of the hydrogen fueling from both the gas puff and recycling. There is a considerable toroidal asymmetry in the H_α emission, with the maximum level of H_α light occurring at the gas puffer. When used with the neutral gas modeling code DEGAS,⁸⁸ the neutral atom density can be unfolded from the H_α emission. Ion Doppler spectroscopy has been implemented to measure the temperature of intrinsic impurity ions in the plasma. The Doppler broadening of oxygen and carbon lines as measured by a 1 meter spectrometer shows that the ion temperature is $\sim 20\text{eV}$ in discharges with a line average density of $1 \times 10^{12} \text{ cm}^{-3}$. This temperature is sufficient to place the ions in the plateau regime.

The response of the plasma to the electrode pulse is described in chapter 4. When the electrode voltage is applied, the floating potential in the plasma changes on the time scale of the electrode voltage, while the electrode current exhibits a large spike before settling to its equilibrium value during the pulse. The plasma flow is observed to evolve on two time scales. One time scale is faster than the Mach probe can measure ($<10\mu\text{s}$) while the other time scale is approximately $300-500\mu\text{s}$. When the electrode current is broken at the end of the electrode pulse,

the electrode voltage, the floating potential, and one component of the flow decay on a time scale of $\sim 30\mu\text{s}$. A second component of the flow decays on a longer time scale of $\sim 200\mu\text{s}$, although the dynamics appear to be too complicated to treat as a simple two time scale decay. The multiple time scales and asymmetry between the rise and the fall are important clues which are used in the modeling.

Chapter 4 also presents data comparing the Mirror and QHS configurations of HSX. Evidence is shown that the viscous damping is reduced in the QHS configuration compared to the Mirror configuration. In particular, the time scales for the flows to evolve are longer in the QHS than the Mirror configuration. There is more steady state flow in the direction of slow damping in the QHS configuration, further supporting the hypothesis that the flow damping is reduced in the QHS configuration compared to the Mirror.

The neoclassical modeling presented in this dissertation will be in Hamada coordinates; it will be necessary to know the Fourier decomposition of $|B|$ in Hamada toroidal and poloidal angles, as well as the complete Hamada basis vector set. The techniques for calculating these quantities are presented in chapter 5. The Hamada spectrum is calculated using a modification⁸⁹ of the technique originally developed to calculate the Boozer spectrum.⁹⁰ Examples of spectra are shown where the quasi-helical symmetry is broken using the auxiliary coil set. One means of breaking the symmetry is to introduce a long wavelength $(n,m)=(4,0)$ mirror term into the spectrum; a second means is to introduce magnetic islands which lead to distortions of the magnetic surfaces.

Chapter 5 also presents an original method for calculating the Hamada basis vectors. Many previous applications of similar neoclassical modeling have used the large aspect ratio basis vectors for a tokamak⁹¹ when modeling a stellarator configuration. The new technique is motivated by the method to calculate $\nabla\psi$ developed by Nemov,⁹² but has been generalized to include calculations of all three basis vectors. The technique involves integration of the lab-frame components of the basis vectors along a field line. A challenging point is to derive the initial

conditions for this integration; the basis vectors must be known at a single point before they can be integrated forward. A method is described to calculate the basis vectors at the outboard symmetry plane based on a comparison between numerical⁹³ and analytic⁹⁴ calculations of the Pfirsch-Schlueter current. Comparisons between the numerically calculated Hamada basis vectors and the large aspect ratio tokamak basis vectors are made, showing that there are some quantities for which the numerical calculation is significantly more accurate for HSX.

A detailed description of the neoclassical modeling is given in chapter 6. The modeling is based on the formulation put forward by Coronado and Talmadge.⁸² This model includes neoclassical parallel viscosity and ion-neutral friction as mechanisms to damp plasma flows. Besides reformulating the model for a more general flux surface label and allowing for a toroidally asymmetric distribution of neutrals, the model has been somewhat modified based on empirical observations. In particular, the original formulation specified the plasma flow and electric field time evolution subject to an externally driven radial current. This model appears to be appropriate for describing the plasma flow and electric field evolution at electrode turn-off, when the solid state switches break the electrode current. Two time scales are derived for the flow relaxation, corresponding to two directions on a flux surface. On the other hand, the floating potential measurements indicate that the rise of the electric field is the driving feature at bias turn-on. A simple new model has been formulated where a quick rise of the electric field drives the flow evolution. This model also predicts two time scales: the externally imposed fast time scale where the electric field is imposed and the \mathbf{ExB} and compensating flows are formed, and a slower "hybrid" time scale for the bootstrap-like portion of the flow to accelerate. In both the spin-up and spin-down, a two time scale evolution of the plasma flow is predicted. A further product of the calculations is the neoclassical radial conductivity. All of these quantities and predictions can be compared to measurements.

Comparisons between the measurements and the neoclassical modeling are the subject of chapter 7. The radial conductivity in HSX appears to be anomalous. The neoclassical

prediction for the radial conductivity is generally a factor of ~ 10 smaller than the measured values. This is in keeping with the results from axisymmetric systems discussed above. The expression for the radial conductivity by Rozhansky and Tendler, motivated by the anomalous radial conductivity in the TUMAN-3 tokamak, appears to fit the HSX data more accurately than the purely neoclassical model.

With respect to the dynamics of the flow rise at bias turn-on, we observe approximate agreement between the spin-up model developed in the modeling and the experimental observations. The time scales are also in agreement with the modeling, both in their radial profile and their density scaling. The directions for flow evolution are roughly in keeping with the models, although some discrepancies exist in this respect.

Considering the decay of the plasma flow after the electrode current is terminated, there is approximate agreement between the neoclassical fast time scale and the measured fast time scale. The measured slow time scales are ~ 10 times faster than the neoclassical prediction. The directions associated with the flow decay cannot be understood from a neoclassical standpoint.

The appendices contain a set of ancillary data which may be useful to the reader of this dissertation or a researcher at HSX. Appendix 1 provides technical details on the design of the H_{α} detectors and the spectrometer system. Appendix 2 provides a compendium of useful data about the different magnetic configurations accessible in HSX. Detailed information is provided there with the goal of allowing the reader to easily design useful experiments involving changes of the magnetic configuration. Appendix 3 gives some details of the ion-neutral collision frequency used in the calculation of the ion-neutral friction in the neoclassical modeling. Appendix 4 provides information on impurity flow measurements made using Doppler spectroscopy. Appendix 5 applies the viscous damping theory of chapter 6 to different configurations of HSX. Appendix 6 provides a derivation of the neoclassical flows expected in an unbiased 3D torus when the heat fluxes are included in the derivation.

-
- ¹ Intergovernmental Panel on Climate Change, Climate Change 2001: Synthesis Report, Summary for Policymakers, available at <http://www.ipcc.ch>.
- ² T.M. Wigley, R. Richels, and J.A Edmonds, *Nature* **379**, 240 (1996)
- ³ J. Onega and G. Van Oost, *Transaction of Fusion Science and Technology* **41**, 3 (2002)
- ⁴ M.I. Hoffert, K. Caldeire, A. Jain, E. Haites, L.D.D. Harvey, S.D. Potter, M.E. Schlessinger, S.H. Schneider, R. G. Watts, T.M. Wigley, and D. Wuebbles, *Nature* **395**, 881 (1998).
- ⁵ M. I. Hoffert, K. Caldeira, G. Benford, D. Criswell, C. Green, H. Herzog, A.K. Jain, J. S. Khesghi, K.S Lackner, J.S. Lewis, H. D. Lightfoot, W. Mannheimer, et al., *Science* **298**, 981 (2002).
- ⁶ R.J. Goldston and P.H. Rutherford, *Introduction to Plasma Physics*, (Institute of Physics Publishing, London, 1995).
- ⁷ R.C. Wolf, *Plasma Phys. Control. Fusion* **45**, R1 (2003).
- ⁸ J. Jacquinot and the JET Team, *Plasma Phys. Control. Fusion* **41**, A13 (1999).
- ⁹ D.F.H. Start, J. Jacquinot, V. Bergeaud, V.P. Bhatnagar, G.A. Cottrell, S. Clement, L-G. Erikson, A. Fasoli, A. Gondhalekar, G. Grosshoeg, et. al., *Phys. Rev. Lett* **80**, 4681 (1998).
- ¹⁰ C. Gormezano, Y.F. Baranov, C.D. Challis, I. Coffey, G. A. Cottrell, A.C. Ekedahl, C. M. Greenfield, A.C. Howman, G.T.A. Huysmans, et. al., *Phys. Rev. Lett.* **80**, 5544 (1998).
- ¹¹ A. Isayama, Y. Kamada, N. Hayashi, T. Suzuki, T. Oikawa, T. Jujita, T. Fukuda, S. Ide, h. Takenaga, K. Ushigusa, T. Ozeki, Y. Ikeda, N. Umdea, et. al., *Nuclear Fusion* **43**, 172 (2003).
- ¹² S.P. Hirshman and D.J. Sigmar, *Nuclear Fusion* **21**, 1079 (1981).
- ¹³ J.D. Callen, *Notes for ECE/Phys/NEED 527: Plasma Confinement and Heating*, U. of Wisconsin, Madison, 1983.
- ¹⁴ K.C. Shaing and E.C. Crume, Jr., *Phys. Rev. Lett.* **63**, 2369 (1989).
- ¹⁵ M.C. Zarnstorff, M.G. Bell, M. Bitter, R.J. Goldston, B. Grek, R.J. Hawryluk, K. Hill, D. Johnson, D. McCune, H. Park, A Ramsey, G. Taylor, and R. Wieland, *Phys. Rev. Lett.* **60**, 1306 (1988).
- ¹⁶ E.A. Lazarus, G.A. Navratil, C.M. Greenfield, E.J. Strait, M.E. Austin, K.H. Burrell, T.A. Casper, D.R. Baker, J.C. DeBoo, E.J. Doyle, et. al., *Phys. Rev. Lett.* **77**, 2714 (1996).

-
- ¹⁷ P.C. Liewer, *Nuclear Fusion* **25**, 543 (1985).
- ¹⁸ J.W. Connor and H.R. Wilson, *Plasma Phys. Control. Fusion* **36**, 719 (1994).
- ¹⁹ B. A. Carreras, *IEEE Transactions on Plasma Science* **25**, 1281 (1997).
- ²⁰ Figure taken from <http://www.iter.org/ITERPublic/ITER/fr2.html>
- ²¹ K.C. Shaing and J.D. Callen, *Phys. Fluids* **26**, 3315 (1983)
- ²² A.A. Galeev, R.Z. Sagdeev, H.P. Furth, M.N. Rosenbluth, *Phys. Rev. Lett.* **22**, 511 (1969).
- ²³ H. E. Mynick and W. N. G. Hitchon, *Nuclear Fusion* **23**, 1053 (1983).
- ²⁴ H.E. Mynick, T.K. Chu, and A.H. Boozer, *Phys. Rev. Lett* **48**, 322 (1982).
- ²⁵ C.D. Beidler and W.N.G. Hitchon, *Plasma Phys. Control. Fusion* **36**, 317 (1994).
- ²⁶ J. Nuhrenberg and R. Zille, *Physics Letters* **114**, 129 (1986).
- ²⁷ J. Nuhrenberg and R. Zille, *Physics Letters A* **129**, 113 (1988).
- ²⁸ P. Merkel, *Nuclear Fusion* **27**, 870 (1987).
- ²⁹ P.R. Garabedian, *Phys. Plasmas* **4**, 1617 (1997).
- ³⁰ M. C. Zarnstorff, L.A. Berry, A. Brooks, E. Fredrickson, G-Y Fu, S. Hirshman, S. Hudson, L-P Ku, E. Lazarus, D. Mikkelson, D. Monticello, et. al., *Plasma Phys. Control. Fusion* **43**, 237 (2001).
- ³¹ B.E. Nelson, R.D. Benson, L.A. Berry, A.B. Brooks, M.J. Cole, P.J. Fogarty, P.L. Goranson, et. al., *Proceedings of the 19th IEEE/IPSS Symposium on Fusion Engineering*, 248 (2002).
- ³² F.S.B. Anderson, A.F. Almagri, D.T. Anderson, P.G. Mathews, J.N. Talmadge, J.L. Shohet, *Fusion Technology* **27**, 273 (1995).
- ³³ A.H. Boozer, *Phys. Fluids* **24**, 1999 (1981).
- ³⁴ J.N. Talmadge, V. Sakaguchi, F.S.B. Anderson, and A.F. Almagri, *Phys. Plasmas* **8**, 5165 (2001).
- ³⁵ C. Deng, D.L. Brower, W.X.Ding, A.F. Almagri, D.T. Anderson, F.S.B. Anderson, S.P. Gerhardt, P. Probert, and J.N. Talmadge, *Rev. Sci. Instrum.* **74**, 1625 (2003).

-
- ³⁶ K.M. Likin, J.N. Talmadge, A.F. Almagri, D.T. Anderson, F.S.B. Anderson, C. Deng, S.P. Gerhardt, and K. Zhai, *Absorption of X-Wave at the Second Harmonic in HSX*, 15th Topical Conference on Radio Frequency Power in Plasmas, 2003.
- ³⁷ J. Shafi, et. al, Proceeding of the 12th International Stellarator Workshop, Madison, Wisconsin, September 27-October 1, 1999.
- ³⁸ F. Wagner et al., Phys. Rev. Letters **49**, 1408 (1982).
- ³⁹ K.H. Burrell, Phys. Plasmas **4**, 1499 (1997).
- ⁴⁰ J.A. Snipes, et.al., Proceedings of the 19th International Conference on Plasma Physics and Controlled Nuclear Fusion Research, October 14-19, 2002, Lyon, France (International Atomic Energy Agency, Vienna, 2002).
- ⁴¹ K. Ida et al., Phys. Rev. Letters **76**, 1268 (1996)
- ⁴² E.J. Synakowski, M.A. Beer, R.E. Bell, K.H. Burrell, B.A. Carreras, P.H. Diamond, E.J. Doyle, D. Ernst, R.J. Fonck, P. Gohil, C.M. Greenfield, et. al., Nuclear Fusion **39**, 1733 (1999).
- ⁴³ Y.B. Kim, P.H. Diamond, H. Biglari, and J.D. Callen, Phys. Fluids B **3**, 384 (1991).
- ⁴⁴ R. Moyer, K.H. Burrell, T.N. Carlstrom, S. Coda, R.W. Conn, E.J. Doyle, P. Gohil, R.J. Groebner, J. Kim, R. Lehmer, W.A. Peebles, M. Porkolab, et. al., Phys. Plasmas **2**, 2397 (1995).
- ⁴⁵ K.H. Burrell, T.N. Carlstrom, S. Coda, E.J. Doyle, P. Gohil, R.J. Groebner, J. Kim, R.A. Moyer, et. al., Plasma Phys. Control. Fusion **38**, 1313 (1996).
- ⁴⁶ R.E. Bell, F.M. Levington S.H. Batha, E.J. Synakowski, and M.C. Zarnstorff, Phys. Rev. Lett. **81**, 1429 (1998).
- ⁴⁷ F. Levington, R.E. Bell, S.H. Batha, E.J. Synakowski, and M.C. Zarnstorff, Phys. Rev. Lett. **80**, 4887 (1998).
- ⁴⁸ E. J. Straight, L.L.Lao, M.E. Mauer, B.W. Rice, T.S. Taylor, K.H. Burrell, M.S. Chu, E.A. Lazarus, T.H. Osborne, S.J. Thompson, and A.D. Turnbull, Phys. Rev. Lett. **75**, 4421 (1995).
- ⁴⁹ C.M. Greenfield, et.al., Phys. Plasmas **7**, 1959 (2000).

-
- ⁵⁰ A.D. Turnbull, M.S. Chu, T.S. Taylor, et. al., Proceedings of the 16th International Conference on Plasma Physics and Controlled Nuclear Fusion Research, October 7-11, 1996, Montreal, Canada (International Atomic Energy Agency, Vienna, 1997).
- ⁵¹ C.M. Greenfield, K.H. Burrell, E.J. Doyle, R.J. Groebner, W.P. West, T.A. Casper, J.C. DeBoo, C. Fenzi, P. Gohil, J.E. Kinsley, et. al., Plasma Phys. Control. Fusion **44**, A123 (2002).
- ⁵² E.J. Straight, et. al., Phys. Plasmas **4**, 1783 (1997).
- ⁵³ K. Ida, M. Osakabe, K. Tanaka, T. Minami, S. Nishimura, S. Okamura, A. Fujisawa, K. Yamakazi, Y. Yoshimure, S. Kubo, R. Akiyama, et. al., Nuclear Fusion **39**, 1649 (1999).
- ⁵⁴ J. Strachan, M. Bitter, A.T. Ramsey, M.C. Zarnstorff, V. Arunasalam, M.G. Bell, N.L. Bretz, R. Budny, C.E. Bush, S.L. Davis, H.F. Dylla, P.C. Efthimion, R.J. Fonck, et. al., Phys. Rev. Lett. **58**, 1004 (1987).
- ⁵⁵ R. Taylor, M.L. Brown, B.D. Freid, H. Grote, J.R. Liberati, G. J. Morlaes, P. Probyl, D. Darrow, and M. Ono, Phys. Rev Lett. **63**, 2365 (1989).
- ⁵⁶ L.G. Askinazi, V.E. Golant, S.V. Lebedev, V.A. Rozhanskij, and M. Tendler, Nuclear Fusion **32**, 271 (1992).
- ⁵⁷ R.R. Weynants, G. Van Oost, G. Bertschinger, J. Boedo, P. Brys, T. Delvigne, K. H. Dippel, F. Durodie, H. Euringer, K.H. Finken, D.S. Grey, et. al., Nuclear Fusion **32**, 837 (1992).
- ⁵⁸ G.S. Kirnev, V.P. Budaev, M.M. Dremin, E.V. Gerasimov, S.A. Grashin, L.N. Khimchenko, S.V. Krilov, Y.D. Pavlov, D.A. Shelukhin, et. al., Plasma Phys. Control. Fusion **45**, 337 (2003).
- ⁵⁹ D.A. Deibold, N. Hershkowitz, J. Pew, J. Sorensen, T. Tanaka, R. Walsh, E.Y. Wang, X. Wang, and G. Winz, Rev. Sci. Instrum **66**, 434 (1995).
- ⁶⁰ R.R. Weynants and G. Van Oost, Plasma Phys. Control. Fusion **35**, B177 (1993).
- ⁶¹ S. Suckewer, H.P. Eubank, R.J. Goldston, E. Hinnov, and N. Sauthoff, Phys. Rev. Letters **43**, 207 (1979).
- ⁶² S. Suckewer, H.P. Eubank, R.J. Goldston, J. McEnerney, N.R. Sauthoff, and H.H. Towner, Nuclear Fusion **21**, 1301 (1981)

-
- ⁶³ R.C. Isler, A.J. Wooten, L.E. Murray, R.A. Langley, J.D. Bell, C.E. Bush, A. Carnevali, P.H. Edmonds, D. P. Hutchinson, et. al., *Nuclear Fusion* **26**, 391 (1986).
- ⁶⁴ W.M. Stacey, and D.J. Sigmar, *Physics of Fluids* **28**, 2800 (1985).
- ⁶⁵ R.P. Seraydarian, K.H. Burrell, N.H. Brooks, R.J. Groebner, and C. Kahn, *Rev. Sci. Instrum.* **57**, 155 (1986).
- ⁶⁶ A. Kallenbach, H.M. Mayer, G. Fussmann, V. Mertens, U. Stroth, O. Vollmer, and the ASDEX Team, *Plasma Phys. Control. Fusion* **33**, 595 (1991)
- ⁶⁷ H. Weisen, M. Von Hellermann, A. Boileau, L.D. Horton, W. Mandl, and H.P. Summers, *Nuclear Fusion* **29**, 2187 (1989)
- ⁶⁸ S. D. Scott, P.H. Diamond, R.J. Fonck, et. al., *Phys. Rev. Lett.* **64**, 531 (1990).
- ⁶⁹ S.D. Scott, V. Arunasalan, C.W. Barnes, M.G. Bell, M. Bitter, R. Boivin, N.L. Bretz, R. Budny, C.E. Bush, A. Cavallo, T.K. Chu, S. A. Cohen, et. al., *Phys. Fluids B* **2**, 1300 (1990).
- ⁷⁰ N. Mattor and P.H. Diamond, *Phys. Fluids* **31**, 1180 (1988).
- ⁷¹ J.S. deGrassie, D.R. Baker, K.H. Burrell, P. Gohil, C.M. Greenfield, R.J. Groebner, and D.M. Thomas, *Nuclear Fusion* **43**, 142 (2003).
- ⁷² K. Nagashima, Y. Koide, and H. Shirai, *Nuclear Fusion* **34**, 449 (1994)
- ⁷³ W.D. Lee, J.E. Rice, E.S. Marmor, M.J. Greenwald, I.H. Hutchinson, and J.A. Snipes, *Phys. Rev. Lett.* **91**, 205003 (2003).
- ⁷⁴ J.A. Snipes, D.J. Campbell, T.C. Hendler, M. Von Hellermann, and H. Weisen, *Nuclear Fusion* **30**, 205 (1990).
- ⁷⁵ A.K. Hansen, A.F. Almagri, D. Craig, D.J. Den Hartog, C.C. Hegna, S.C. Prager, and J.S. Sarff, *Phys. Rev. Lett.* **85**, 3408 (2000).
- ⁷⁶ R.R. Weynants and R.J. Taylor, *Nuclear Fusion* **30**, 945 (1990).
- ⁷⁷ V. Rozhansky, and M. Tendler, *Phys. Fluids B* **4**, 1878 (1992).
- ⁷⁸ J. Cornelis, R. Sporken, G. Van Oost, and R.R. Weynants, *Nuclear Fusion* **34**, 171 (1994).

-
- ⁷⁹ A.F. Almagri, J.T. Chapman, C.S. Chaing, D. Craig, D.J. Den Hartog, C.C. Hegna, and S.C. Prager, *Phys. Plasmas* **5**, 3982 (1998).
- ⁸⁰ S. Sudo, Y. Takeiri, H. Zushi, F. Sano, K. Itoh, K. Kondo, and A. Iiyoshi, *Nuclear Fusion* **30**, 314 (1997).
- ⁸¹ J.N. Talmadge, B.J. Peterson, D.T. Anderson, F.S.B. Anderson, H. Dahi, J.L. Shohet, M. Coronado, K.C. Shaing, et. al., *Proceedings of the 15th International Conference on Plasma Physics and Controlled Fusion Research (Seville, 1994)*, IAEA, Vienna, **1** (1995) 797.
- ⁸² M. Coronado and J.N. Talmadge, *Phys. Fluids B* **5**, 1200 (1993).
- ⁸³ M. Hirsh, P. Grigull, H. Wobig, J. Kisslinger, K. McCormick, M. Anton, J. Baldzuhn, S. Fiedler, et. al., *Plasma Phys. Control. Fusion* **42**, A231 (2000).
- ⁸⁴ F. Wagner, J. Baldzuhn, R. Brakel, R. Burhenn, V. Erckmann, T. Estrada, P. Grigull, H. J. Hartfuss, G. Herre, M. Hirsch, J. V. Hofmann, R. Jaenicke, A. Rudyj, U. Stroth and A. Weller, *Plasma Phys. Control. Fusion* **36**, A61 (1994).
- ⁸⁵ H. Wobig and J. Kisslinger, *Plasma Phys. Control. Fusion* **43**, 823 (2000).
- ⁸⁶ F. Sano, T. Mizuuchi, K. Nagasaki, H. Okada, S. Kobayashi, K. Kondo, K. Hanatani, Y. Nakamura, et. al., *Proceedings of the 14th Stellarator Workshop, Greifswald, Germany 2003*.
- ⁸⁷ C.S. MacLatchy, C. Boucher, D.A. Poirier, and J. Gunn, *Rev. Sci. Instrum.* **63**, 3923 (1992).
- ⁸⁸ D.B. Heifetz, et. al., *J. Comp. Phys.* **46**, 309 (1982).
- ⁸⁹ Private communication with J.N. Talmadge
- ⁹⁰ G. Kuo-Petravic, A. H. Boozer, J.A. Rome, and R.H. Fowler, *Journal of Computational Physics* **51**, 261 (1983).
- ⁹¹ M. Coronado and J. Galindo Trejo, *Phys. Fluids B* **2**, 530 (1990).
- ⁹² V.V.Nemov, *Nuclear Fusion* **28**, 1727 (1988).
- ⁹³ V.V. Nemov, *Nuclear Fusion* **30**, 927 (1990).
- ⁹⁴ M. Coronado and H. Wobig, *Phys. Fluids B* **4**, 1294 (1992).